OPEN ACCESS

University of Dundee

University of Dundee

The stability and redox mechanisms of Ni-rich NMC cathodes

Banerjee, Hrishit; Grey, Clare P.; Morris, Andrew J.

DOI:
10.26434/chemrxiv-2024-bjzbt

Publication date:
2024

Licence:
CC BY-NC-ND

Document Version
Publisher's PDF, also known as Version of record

Link to publication in Discovery Research Portal

Citation for published version (APA):
Banerjee, H., Grey, C. P., & Morris, A. J. (2024). *The stability and redox mechanisms of Ni-rich NMC cathodes: Insights from first-principles many-body calculations*. ChemRxiv. https://doi.org/10.26434/chemrxiv-2024-bjzbt

General rights
Copyright and moral rights for the publications made accessible in Discovery Research Portal are retained by the authors and/or other copyright owners and it is a condition of accessing publications that users recognise and abide by the legal requirements associated with these rights.

Take down policy
If you believe that this document breaches copyright please contact us providing details, and we will remove access to the work immediately and investigate your claim.

Download date: 04. Jul. 2024

The stability and redox mechanisms of Ni-rich NMC cathodes: Insights from first-principles many-body calculations

Hrishit Banerjee,*,†,‡,¶,§ Clare P. Grey,*,†,¶ and Andrew J. Morris*,‡,¶

†*Yusuf Hamied Department of Chemistry, University of Cambridge, Lensfield Road, CB2 1EW, Cambridge, Cambridgeshire, UK.*

‡*School of Metallurgy and Materials, University of Birmingham, Birmingham, UK*

¶*The Faraday Institution,Quad One, Harwell Science and Innovation Campus, Didcot, UK.*

§*School of Science and Engineering, University of Dundee, Nethergate, DD1 5LR, Scotland, UK*

E-mail: hb595@cam.ac.uk; cpg27@cam.ac.uk; a.j.morris.1@bham.ac.uk

Abstract

Ni-rich $LiNi_aMn_bCo_cO_2$ (NMC) cathodes undergo a series of degradation reactions, a prominent one being oxygen loss from the surface of the NMC particles, this process being more pronounced as Ni content is increased and at high voltages. Our first-principles study examines the redox behavior of transition metals and O in Ni-rich NMC cathodes as a function of (de)lithiation. We use *ab initio* multiple scattering, density-functional theory (DFT) based core-loss spectroscopy, and dynamical mean-field theory (DMFT) to give a many-body treatment of both dynamic and static correlations. Despite Ni, Mn, and Co K-edges calculated using ab initio multiple scattering based on Green's functions showing an excellent match with experimentally obtained X-ray absorption near-edge spectra (XANES), we demonstrate that the ionic model

https://doi.org/10.26434/chemrxiv-2024-bjzbt **ORCID:** https://orcid.org/0000-0001-7852-497X Content not peer-reviewed by ChemRxiv. **License:** CC BY-NC-ND 4.0

of ascribing shifts in the XANES spectra to changes in metal oxidation states is inappropriate. We show that in these cases, which are characterised by strong covalency between the transition metal and oxygen, DMFT calculations based on Wannier projections are essential to calculate charges and hence assign oxidation states accurately. Due to the corresponding charge transfer from O p to Ni d, a ligand hole forms on O in Ni-rich regions. The individual Ni charge remains fairly constant throughout the charging/discharging process, particularly in Ni-rich environments in the material. In contrast, O has dual redox behavior, showing greater involvement in redox in Ni-rich regions while showing negligible redox involvement in Ni-poor regions. The Ni-O covalent system starts participating in redox around a state of delithiation of $\sim$17%, which represents, in our system, the beginning of charge. Contrary to previous DFT calculations, we show that Co oxidation does not occur at the very end of charge but rather starts at an earlier state of delithiation of $\sim$67%. The dual behaviour of O in terms of participation in the redox process helps explain the overall higher relative stability of lower Ni content NMCs compared to Ni-rich NMCs or $LiNiO_2$ in terms of O loss and evolution of singlet oxygen.

Introduction

Lithium-ion batteries (LIBs)[1,2] have brought about a revolution in portable electronic devices due to their outstanding performance. They are now also key to enabling the ubiquitous use of electric vehicles (EV). Among several factors affecting the performance of LIBs, the cathode material is the most critical component as it primarily regulates both the LIB's specific energy density and strongly impacts the long-term capacity retention of the LIB. Recently, lithiated transition metal (TM) oxides of the form $Li_x[Ni_aMn_bCo_c]O_2$, where a, b, c are fractions of Ni, Mn, and Co respectively ($a+b+c=1$), known as NMCs, have emerged as a promising family of cathode materials for LIBs.[3–12]

The demand for high energy density materials has led to extensive research efforts to

https://doi.org/10.26434/chemrxiv-2024-bjzbt **ORCID:** https://orcid.org/0000-0001-7852-497X Content not peer-reviewed by ChemRxiv. **License:** CC BY-NC-ND 4.0

discover novel NMC compositions and to optimise their electrochemical performance. A particular focus has been to identify materials with high nickel content (so-called "Ni-rich" NMC materials (a > 0.5)[3,6–8,10,13–15]) as they can provide higher specific capacity within the same voltage window and decrease dependence on scarce, geographically-concentrated, and costly cobalt.[16,17]

While the increased capacity of these materials is a highly desirable property from a technological standpoint, the thermal and structural stability of Ni-rich cathodes decreases with Ni content, for reasons that are still poorly understood.[4,18–27] There is still extensive debate concerning the involvement of different redox species in the redox process.[28–30]

Taking the example of $LiNiO_2$ (LNO), one origin of the instability lies in the pronounced oxidation of O during delithiation: for LNO, NiO_2, and the rock salt (RS) NiO, density-functional theory (DFT) and state-of-the-art dynamical mean-field theory (DMFT) calculations based on maximally localized Wannier functions yield a Ni charge state of $\sim +2$, with the O charge state, not the Ni one, varying between $\sim$ -2 (NiO), $\sim$-1.5 ($LiNiO_2$), and $\sim$-1 (NiO_2).[31] This study also investigated degradation mechanisms, using *ab initio* molecular dynamics simulations showing that the loss of oxygen from the (012) surface of delithiated $LiNiO_2$, (i.e., NiO2) occurs via two surface $O^{\cdot -}$, radicals combining to form a peroxide ion, and the peroxide ion being oxidized to form O_2, leaving behind two O vacancies and two O^{2-} ions. Release of $^1O_2$ is dictated via the singlet ground state of the peroxide ion and spin conservation. Thus, when cycling the NMC parent compound LNO, O redox plays an important role. The question that this current article seeks to address is: how does Mn and Co substitution for LNO affect TM and O oxidation as a function of state-of-charge (SOC) and how is this affected by cation ordering. Specifically, to elucidate the relative stabilities of the different Ni-rich NMC cathodes towards O loss[22] and $^1O_2$ generation,[22] it is imperative to understand the involvement of the different redox species in the redox processes during cycling.

One method that the experimental community uses to track oxidation state are the

https://doi.org/10.26434/chemrxiv-2024-bjzbt **ORCID:** https://orcid.org/0000-0001-7852-497X Content not peer-reviewed by ChemRxiv. **License:** CC BY-NC-ND 4.0

shifts of TM K-edges in X-ray absorption near edge structure (XANES) spectra, and using these spectra it has been claimed that the major redox activity on delithiation is centred on Ni and Co, while Mn and O play the role of mere spectators.[29] The assignment of oxidation states based on TM K edge shifts depends heavily upon two factors: namely the reference to standard XANES edges where oxidation states are presumed to be well known, and the (often implicit) assumption of an ionic point-charge model for the TM ions. However, without proper first principles modelling of such spectra along with accurate charge analysis, this approach may be misleading, particularly in highly covalent and strongly correlated systems. The inaccuracies may stem from wrong assignments of the reference standards themselves, as well as the large covalency between TM and O atoms, which are assumed to be ionic. In particular, this latter assumption is not supported by DFT-based studies of these materials,[28] which highlight the strong covalency of Ni and O in NMCs. For example, strong covalency between Ni *d*- and O *p*-orbitals in Ni-rich cathodes has, for example, been previously demonstrated by means of Integrated Crystal Orbital Population (ICOHP) calculations.[28,30,32] Yet, whilst clearly demonstrating large covalency, these studies still resorted to the standard ionic picture of "formal" oxidation states. These "formal charges" are useful in terms of accounting for changes in the overall redox state of the material, but are less useful in understanding how the charges are distributed. Hence, in this article, we will discuss only changes in occupancy of the different Ni *d* or O *p* orbitals.

In another combined experimental and theoretical study, even though charge calculations from Bader analysis also show changes in the charge states of O upon cycling,[29] this study also adheres to "nominal" ionic oxidation states despite evidence pointing towards a covalent character of TM-O bonds. Thus, a conclusive answer is still needed when it comes to the question of accurate determination charge/oxidation states, and associated redox processes: whilst O plays a crucial role in the structural and thermal stability of LNO,[31] the possible involvement of O in commercially relevant cathodes like NMCs is still an open question.

In first principles studies, assigning oxidation/charge states is often carried out based

https://doi.org/10.26434/chemrxiv-2024-bjzbt **ORCID:** https://orcid.org/0000-0001-7852-497X Content not peer-reviewed by ChemRxiv. **License:** CC BY-NC-ND 4.0

on magnetic moments/bader charges obtained from ground-state DFT calculations. Thus to understand the redox processes of Ni-rich NMCs, and determine the oxidation/charge states of different species correctly it is imperative to first have a correct description of the ground-state electronic structure of the pristine (fully lithiated) materials. The electronic ground states of Ni-rich NMC cathodes such as $LiNi_{0.6}Mn_{0.2}Co_{0.2}O_2$ (NMC-622) or $LiNi_{0.8}Mn_{0.1}Co_{0.1}O_2$ (NMC-811) are semiconducting[33] with conductivity of the order of $10^{-4} - 10^{-3}$ S/cm for Ni-rich NMCs and $\sim 10^{-7}$ S/cm for $LiNi_{0.33}Mn_{0.33}Co_{0.33}O_2$ (NMC-111). Thus, one would expect a larger electronic band gap in NMC-111 compared to Ni-rich NMCs based on these conductivity measurements. However, even the band gap and ground-state electronic structure are not well described within DFT: first principles DFT studies employing either local Generalised Gradient Approximation (GGA), with on-site corrections for the correlation energy in the form of the addition of static Hubbard U or semi-local (meta-GGA) functionals, report a ferromagnetic half-metallic state[28,30,32] for NMCs. Other studies have carried out calculations assuming an antiferromagnetic configuration to obtain such a small band-gap semiconducting state, without a comparison of the derived total energies with ferromagnetic/ferrimagnetic states or a clear steer from experiment concerning such AFM ordering in a material.

The magnetic ground states of pristine Ni-rich NMCs are, however, highly sample-dependent and debatable at best.[34] Magnetic measurements by Mukherjee *et al.*[34] on two samples of NMC-811 having composition $Li_{1-x}Ni_{0.9+x-y}Mn_yCo_{0.1}O_2$, with x = 0.025, y = 0.120 for Sample 1 and x = 0.002, y = 0.094 for sample 2 corresponding to different concentrations of magnetic ions and excess Ni^{2+} in the Li^+ layers reveal a transition at 8 K for both their samples, but the Zero field cooled (ZFC)-Field cooled (FC) curves deviate at very different temperatures: T_{ZFC-FC} = 64 K for Sample 1 and 122 K for Sample 2. Another experimental study observed a ferrimagnetic quasi long-range order and a 2D spin glass-like behavior on cooling below $T_C \sim 70K$, followed by a complete spin frustration in three dimensions below 30 K,[35] with anti-site defects strongly controlling short and long-range

https://doi.org/10.26434/chemrxiv-2024-bjzbt **ORCID:** https://orcid.org/0000-0001-7852-497X Content not peer-reviewed by ChemRxiv. **License:** CC BY-NC-ND 4.0

ordering. Earlier work by Chernova *et al.*[9] that in NMCs, specifically $LiNi_{0.45}Mn_{0.45}Co_{0.1}O_2$ and $LiNi_{1/3}Mn_{1/3}Co_{1/3}O_2$ - no long-range magnetic order is established and instead large magnetically ordered clusters are formed. They demonstrate that with increasing Co^{3+} content the amount of interslab Ni^{2+} ions decreases; Ni^{3+} ions coupled by 180° exchange interactions form smaller clusters due to dilution with nonmagnetic Co^{3+} ions, which in $LiNi_{0.45}Mn_{0.45}Co_{0.45}O_2$ results in the cluster-glass behavior. A further increase in the Co content makes cluster formation even less probable due to significant dilution of the Ni/Mn lattice with nonmagnetic Co^{3+} ions. This results in the spin-glass transitions at 10 and 7 K found in $LiNi_{0.4}Mn_{0.4}Co_{0.45}O_2$ and $LiNi_{1/3}Mn_{1/3}Co_{1/3}O_2$, respectively.

Owing to the fact that the magnetic ground state of Ni-rich NMCs are highly debatable even in experimental studies, the idea of assigning oxidation states based on magnetic moments obtained from DFT is clearly inadequate when it comes to NMCs. Beyond DFT, many-body methods like the *GW* approximation (GWA), random-phase approximation (RPA), and/or DMFT used in conjunction with DFT have in recent times shown excellent match with experimental studies of other strongly correlated systems[36–39] in terms of the description of electronic band gaps, nature of correlated metallic states, accurate calculation of charge states or reproduction of PES/XPS and XAS lineshapes of battery materials which have strongly correlated open *d* shells. Although computationally expensive, recent developments in correlated methods like DMFT or GWA have made the study of cathode materials at various states of charge possible.[40] The advantage of using DMFT is twofold: first, it allows the self-interaction correction which is missing in DFT to be included, which provides the local (momentum independent) self-energy; second, it also allows a paramagnetic state at finite temperature to be calculated using the continuous-time quantum Monte Carlo solver. DMFT calculations have, to date, provided phase diagrams showing Mott transitions in cathode materials like $LiCoO_2$ (LCO)[41] and $LiMnO_2$ (LMO)[40] and have explored the phases and structural stability of these materials as a function of state-of-charge. Marianetti *et al.*[41] explain the phase stability of LCO, which is not captured correctly by DFT, which predicts

https://doi.org/10.26434/chemrxiv-2024-bjzbt **ORCID:** https://orcid.org/0000-0001-7852-497X Content not peer-reviewed by ChemRxiv. **License:** CC BY-NC-ND 4.0

a phase separation into charge-ordered states at 50% and 100% states of charge which are in disagreement with experiments. This tendency is not seen in DFT+DMFT, which matches with experimental results. Thus DFT+U is wrong even in moderately correlated systems like LCO, when it comes to critical aspects of electronic structure. Banerjee et al[40] predict charge disproportionated states in $Li_{0.5}MnO_2$, which are again not captured by DFT, but are at the origin of transition pathways leading to structural transformations to spinel state.

DMFT calculations based on Wannier function basis sets derived from DFT have made accurate charge determination possible in $LiNiO_2$,[31] and demonstrated the significant involvement of O in the redox process of charging/discharging. Although some involvement of O was seen at the DFT level based on the calculation of Bader charges, accurate determination of ligand hole states with the calculation of charge states to a high precision was only possible based on the integration of Green's functions derived from DMFT calculations. *Ab initio* multiple scattering calculations based on Green's functions implemented through the GW_0 approximation for TM XANES K edges have shown excellent agreement with experimental studies for LNO.[31]

In this article, we examine the redox behaviour of Ni-rich NMCs with varying Ni contents using primarily beyond-DFT methods. The most popular and now commercial, Ni-rich cathode material is NMC-811 comprising of 80% Ni, 10% Mn and 10% Co[3,6–8,10,13–15] is studied. We use a combination of theoretical spectroscopy, both a hybrid-DFT-based pseudopotential method, as well as a Green's function based *ab initio* multiple scattering method to obtain an accurate description of the TM XANES edges of Ni, Mn and Co. We carry out an accurate determination of charges on ions from DMFT calculations. We observe changes in the correlated spectral functions as a function of delithiation, which show the involvement in redox processes of the different TM ions. Specifically, we see a clear transition in the involvement of O in the redox process as a function of Ni content, which correlates with the stability of the cathodes.

https://doi.org/10.26434/chemrxiv-2024-bjzbt **ORCID:** https://orcid.org/0000-0001-7852-497X Content not peer-reviewed by ChemRxiv. **License:** CC BY-NC-ND 4.0

Computational Methods

DFT Calculations Our DFT calculations for structural relaxation and electronic ground-state self-consistent field (SCF) were carried out in a plane-wave basis with projector-augmented wave (PAW) potentials[42] as implemented in the Vienna Ab-initio Simulation Package (VASP).[43,44] For our DFT+DMFT calculations, we use the full-potential augmented plane-wave basis as implemented in the WIEN2K code.[45]

In all our DFT relaxation calculations, we chose as exchange-correlation functional GGA, implemented following the Perdew Burke Ernzerhof (PBESol) prescription for solids.[46] The DFT+U calculations were carried out in the form of PBE+U. The value of U at the TM sites in the GGA+U scheme was varied between 5 and 7 eV, with Hund's exchange J_H of 0.5-0.75 eV, depending on the TM ion being considered. Hybrid functional calculations were carried out following the prescription of Heyd-Scuseria-Ernzerhof (HSE). The functional used in hybrid calculation can be mathematically expressed as

$$E_{XC}^{HSE}(\sigma) = \alpha E_X^{HF,SR}(\sigma) + (1-\alpha)E_X^{PBE,SR}(\sigma) + E_X^{PBE,LR}(\sigma) + E_C^{PBE}$$

which is the range-separated HSE functional, where α is the fraction of Fock exchange and σ is an adjustable parameter controlling the short-rangeness of the interaction. Here $E_X^{HF,SR}$ denotes the short-range Hartree Fock (HF) exchange functional, $E_X^{PBE,SR}$ denotes the short-range PBE exchange functional, $E_X^{PBE,LR}$ indicates the long-range PBE exchange functional, and E_C^{PBE} refers to the correlation functional as given by PBE. The standard value of $\sigma = 0.2$ (referred to as HSE06) along with the standard value of $\alpha = 0.25$ was used.

For ionic relaxations using the VASP package, the internal positions of the atoms, as well as the lattice parameters, were allowed to relax until the forces became less than 0.005 eV/Å. An energy cutoff of 600 eV and a 6×6×2 Gamma-centred k-points mesh provided good convergence of the total energy.

For the WIEN2K calculations, we used the largest possible muffin-tin radii, and the plane-

https://doi.org/10.26434/chemrxiv-2024-bjzbt ORCID: https://orcid.org/0000-0001-7852-497X Content not peer-reviewed by ChemRxiv. License: CC BY-NC-ND 4.0

wave cutoff was defined by $R_{\min} \cdot K_{\max} = 8$, where $R_{\min}$ is the muffin-tin radius of the O atoms. The consistency between the VASP and WIEN2K ground state results has been cross-checked.

Prediction of XAS using hybrid functional calculations X-ray absorption spectra for the O K edge were calculated with VASP6 using PAW with an energy cutoff of 600 eV. A core hole was introduced in the $1s$ state of O. The HSE06 functional was chosen with 25% Fock exchange to have a better description of the non-local nature of O states as well as the correct semiconducting ground state.

F_{eff} Calculations for prediction of XANES for strongly correlated TM In our study, we employed the FEFF10 code for the *ab initio* calculation of K-edge XANES for the transition metals. The X-ray absorption spectra of transition metals are commonly dominated by atomic multiplet interactions arising from electron correlation.[47] FEFF employs Green's formulation of the multiple scattering theory to compute the spectra.[48,49] The X-ray absorption μ is calculated in a manner similar to Fermi's golden rule when written in terms of the projected photo-electron density of final states or the imaginary part of the one-particle Green's function, $G(r, r'; E)$. In terms of the Green's function, $G(r, r'; E)$, the absorption coefficient, μ, from a given core level c is given by ref.[50]

$$\mu = -\frac{1}{\pi} Im \langle c | \epsilon_r \dot{G}(r, r'; E) \epsilon_{r'} | c \rangle$$

with the Green's function, $G(r, r'; E)$ given by

$$G(r, r'; E) = \sum_f \frac{\Psi_f(r) \Psi_f^*(r')}{E - E_f + i\Gamma}$$

where Ψ_f are the final states, with associated energies E_f and net lifetime Γ, of a one-particle Hamiltonian that includes an optical potential with appropriate core hole screening. The

https://doi.org/10.26434/chemrxiv-2024-bjzbt **ORCID:** https://orcid.org/0000-0001-7852-497X Content not peer-reviewed by ChemRxiv. **License:** CC BY-NC-ND 4.0

FEFF code computes the full propagator G incrementally using matrix factorization and uses the spherical muffin-tin approximation for the scattering potential. For self-consistent potential calculations required in the XANES calculation for the Fermi level E_0 estimation a large value of rfms1 of 9 Åwas chosen to have a large number of atoms included in the self-consistent potential calculations. Full multiple scattering (FMS) is required in the XANES calculation as the multiple scattering (MS) expansion's convergence might not be stable in the XANES calculation. A large rfms value of 11 Åwas considered for proper convergence. The Hedin-Lundqvist self-energy was chosen for the exchange-correlation potential model used for XANES calculation. The random phase approximation (RPA) is used to approximate the core-hole interactions in our K-edge XANES calculations.

DMFT Calculations DMFT calculations were performed using the DFTTools module[51–53] of the Toolbox for Research in Interacting Quantum Systems (TRIQS) libraries.[54] We perform DMFT calculations in a basis set of maximally localised Wannier functions (MLWF) constructed using Wannier90[55] and the wien2wannier[56] interface. Projective Wannier functions as implemented in the dmftproj module of TRIQS were employed to crosscheck the results and also to calculate the initial occupancy of the correlated orbitals. The DMFT calculations in both MLWF and projective Wannier functions basis have been found to yield consistent results. A full projection window of $-8\,\mathrm{eV}$ to $+3\,\mathrm{eV}$ was chosen. A dp model was chosen for Ni d + O p states which are strongly covalent and have a large overlap between d and p bands, to accurately describe possible charge transfer phenomena, whereas a d model was chosen for Co d and Mn d states which have much less overlap with O p bands, and hence negligible charge transfer. Any hybridisation in the case of the d only models is taken care of by the contributions of O p on the tails of the Wannier functions. The Anderson impurity models, constructed by mapping the many-body lattice problems to local problems of impurity interacting with bath was solved using the continuous-time quantum Monte Carlo algorithm in the hybridization expansion[57] as implemented in the TRIQS/cthyb package.[58]

https://doi.org/10.26434/chemrxiv-2024-bjzbt **ORCID:** https://orcid.org/0000-0001-7852-497X Content not peer-reviewed by ChemRxiv. **License:** CC BY-NC-ND 4.0

For each DMFT step, 1280000 cycles of warmup steps and 12800000 cycles of measures were performed for the quantum Monte Carlo calculations. We performed one-shot DFT+DMFT calculations, using a fully localised limit (FLL) type double-counting correction.[59]

The interaction part of the fully rotationally invariant Kanamori Hamiltonian using the density-density, spin-flip and pair-hopping interactions. is given by,

$$H = \frac{1}{2} \sum_{(i\sigma)\neq(j\sigma')} U_{ij}^{\sigma\sigma'} n_{i\sigma} n_{j\sigma'} - \sum_{i\neq j} J a_{i\uparrow}^{\dagger} a_{i\downarrow} a_{j\downarrow}^{\dagger} a_{j\uparrow} + \sum_{i\neq j} J a_{i\uparrow}^{\dagger} a_{i\downarrow}^{\dagger} a_{j\downarrow} a_{j\uparrow},$$

where i and j represent orbital indices. U is the Coulomb repulsion between two electrons with opposite spin in the same orbital. Orbital rotational symmetry is imposed by setting $V = U - 2J$, where J is the Hund's coupling, which lowers the energy of a configuration with different orbitals ($i \neq j$), and parallel spins $\sigma = \sigma^{'}$. $a^{\dagger}$ and a are the creation and annihilation operators respectively.

For our DMFT calculations, we used U values ranging from 5 to 7 eV and $J_H = 0.5 - 0.75$ eV depending on the TM ion in question. We obtained real-frequency spectra using the maximum-entropy method of analytic continuation of Green's functions as implemented in the TRIQS/MAXENT application.[60] We carried out Multi-impurity DMFT calculations in a computationally fast and tractable way.[40] Delithiating the system results in the formation of crystallographically inequivalent Ni sites in the NMC supercell, which requires solving multi-impurity problems, involving solutions of extremely large density matrices, which is computationally expensive. To make the problem tractable, MLWF were constructed for all structurally inequivalent sites, however, each inequivalent site was solved as a single-impurity problem interacting through the bath with the other inequivalent sites by virtue of the constructed MWLF. This method works well for strongly localised impurity problems and makes accurate calculations at low temperatures converge faster with much less noise, avoiding the statistical sign problem.[40]

https://doi.org/10.26434/chemrxiv-2024-bjzbt **ORCID:** https://orcid.org/0000-0001-7852-497X Content not peer-reviewed by ChemRxiv. **License:** CC BY-NC-ND 4.0

Results

Crystal Structure

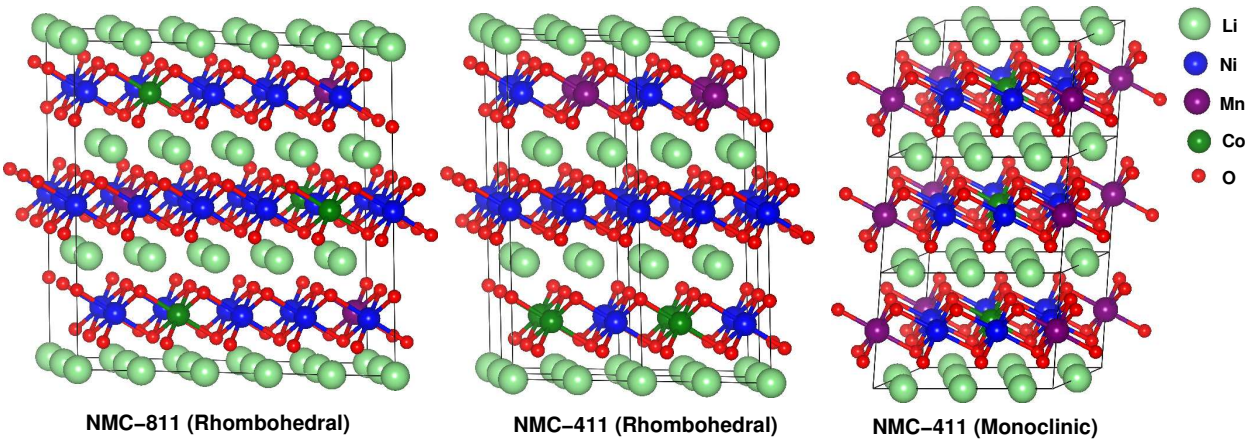

Figure 1: Crystal Structures of NMC-811 and NMC-411. The left panel shows the crystal structure of NMC-811 constructed based on the rhombohedral LNO cell by making a 5×2×1 supercell and replacing in each layer 2 Ni by 1 Mn and 1 Co atom. The middle panel shows the NMC-411 constructed on the 2×1×1 supercell of rhombohedral LNO, replacing 1 Ni in the top layer by Mn and 1 Ni in the bottom layer by Co. The right panel shows a monoclinic NMC-411 constructed by making a 2×2×1 supercell of Li_2MnO_3 and replacing the excess Li in the Ni layer by Mn and 1 Ni in the Ni layer by Co. All the structures are relaxed using PBESol functional and none of the structures show the presence of any Jahn Teller distortion. The two different NMC-411 structures allow us to investigate the effect of (de)clustering among the Mn and Co dopant atoms.

We begin with the details of how the NMC unit cells were built. We consider Ni-rich NMCs with fractions of Ni more than 50%. X-ray diffraction (XRD) shows NMC-811 crystallises into the rhombohedral $R\bar{3}m$ space group[13] with cation disorder, where the TM sites have fractional occupancies. Hence to carry out theoretical calculations, we need to make supercells of this structure and explore the effects of (de-)clustering of TM ions within the disordered structure.

A simulation cell containing 120 atoms is constructed with a TM ratio of 8:1:1 with a 5×2×1 supercell of the rhombohedral disordered experimental NMC-811 primitive cell. In each layer, we replace two Ni atoms with one Mn and one Co respectively, as shown in the left panel of Fig. 1. Whilst it is possible to perform electronic structure calculations using

https://doi.org/10.26434/chemrxiv-2024-bjzbt ORCID: https://orcid.org/0000-0001-7852-497X Content not peer-reviewed by ChemRxiv. License: CC BY-NC-ND 4.0

this large supercell within DFT, it is computationally intractable for many-body (DMFT) calculations.

The smaller supercells necessary to make the DMFT calculations tractable naturally cause an underestimation of the TM site disorder. To this end, we have built two smaller supercells based on NMC-411 (which has the chemical formula, $LiNi_{0.67}Mn_{0.16}Co_{0.16}O_2$) with different TM site disorder, leading to either a rhombohedral or a monoclinic supercell. Note that this composition is intermediate between that of another industrially relevant NMC cathode material NMC-622 and NMC-811.

The rhombohedral NMC-411 model is constructed from the smaller 2×1×1 supercell of the $R\bar{3}m$ disordered experimental NMC-811 primitive cell. In this case, we replace 2 Ni (out of 6 total) with 1 Mn and 1 Co respectively in the top and bottom layers. DFT is used to verify the electronic structure of these NMC-411 supercells against our NMC-811 model. The rhombohedral NMC-411 supercell allows us to investigate separately the physics of Ni-rich and Ni-poor regions of model NMC cathodes at the many-body physics level. This particular model has Ni-rich regions and regions where Ni is sited at sites next to Co or Mn with the Ni-O-Ni superexchange replaced by Ni-O-Mn/Co superexchange. Our second model, constructed to avoid clustering of Co and Mn, is a 2×2×1 supercell of a monoclinic Li_2MnO_3 structure. We replace the excess Li in the TM layers with either Ni or Co or Mn keeping the same fraction of 4 Ni to 1 Co and 1 Mn, carefully avoiding any clustering effects of Mn and Co dopant atoms, while maintaining a NMC-411 stoichiometry. Both rhombohedral and monoclinic NMC-411 are shown in Fig. 1.

For completeness, we considered other structures with different NMC fractions to check the accuracy of different functionals in predicting the correct ground state depending on the percentage of Ni, the effect of clustering, and the effect of breaking symmetry. Since this is not central to the paper we show this in SI, for $LiNi_{0.5}Mn_{0.33}Co_{0.16}O_2$ (NMC-321), $LiNi_{0.5}Mn_{0.3}Co_{0.2}O_2$ (NMC-532), $LiNi_{0.77}Mn_{0.11}Co_{0.11}O_2$ (NMC-711), $LiNi_{0.83}Mn_{0.083}Co_{0.083}O_2$ (NMC-10-1-1), for rhombohedral structures, and

https://doi.org/10.26434/chemrxiv-2024-bjzbt **ORCID:** https://orcid.org/0000-0001-7852-497X Content not peer-reviewed by ChemRxiv. **License:** CC BY-NC-ND 4.0

$LiNi_{0.75}Mn_{0.125}Co_{0.125}O_2$ (NMC-611) for a JT distorted monoclinic structure, derived from a monoclinic JT distorted LNO.

Even though the physics of Ni-rich NMCs is very different from NMC-111 we will use the NMC-111 system ($LiNi_{0.33}Mn_{0.33}Co_{0.33}O_2$) to benchmark our DMFT charges with experimentally determined oxidation states since this is an extremely well-studied system in terms of XANES spectra and corresponding determination of oxidation states.[61] The NMC-111 supercell is a $3 \times 3 \times 1$ supercell of the disordered NMC-811 primitive unit cell and is constructed in such a way that there is no clustering effect of TM ions.

Finally, we construct a RS supercell from the prototypical RS structure of NiO (with space group $Fd\bar{3}m$) so as to benchmark and compare the redox states obtained while cycling as done by Genreith Schriever et al.[31] This cell comprises 12 Ni and 12 O atoms by replacing 1 Ni with Mn and 1 with Co, to yield a composition $Ni_{0.83}Mn_{0.083}Co_{0.083}O$ (see SI figure 1).

All the structures were relaxed in the pristine and various delithiated states using the PBESol functional within VASP. PBESol yields a better accuracy for lattice constants for solids compared to standard PBE.[62,63] The symmetry of the lattice was fixed in each case and the lattice constants and ionic positions were relaxed to minimize both external pressure and forces on the ions.

Ground-state electronic structure

In this section, we examine the ground-state electronic structure of the rhombohedral NMC-811, the rhombohedral NMC-411 and the monoclinic NMC-411 models using the HSE06 functional. For each of our models, the DOS look similar to each other within the same level of theory, however, the atomically-resolved partial density of states (PDOS) from our DFT calculations using the PBESol+U functional does indeed predict a half-metallic ground state, as shown for all three structures in Fig. 2, consistent with previous theoretical work.[28] In better agreement with experiments, for all three models, the HSE06 functional with 25 % Fock exchange shows an insulating ground state with a small band gap of 0.6eV, 0.3eV, and

https://doi.org/10.26434/chemrxiv-2024-bjzbt **ORCID:** https://orcid.org/0000-0001-7852-497X Content not peer-reviewed by ChemRxiv. **License:** CC BY-NC-ND 4.0

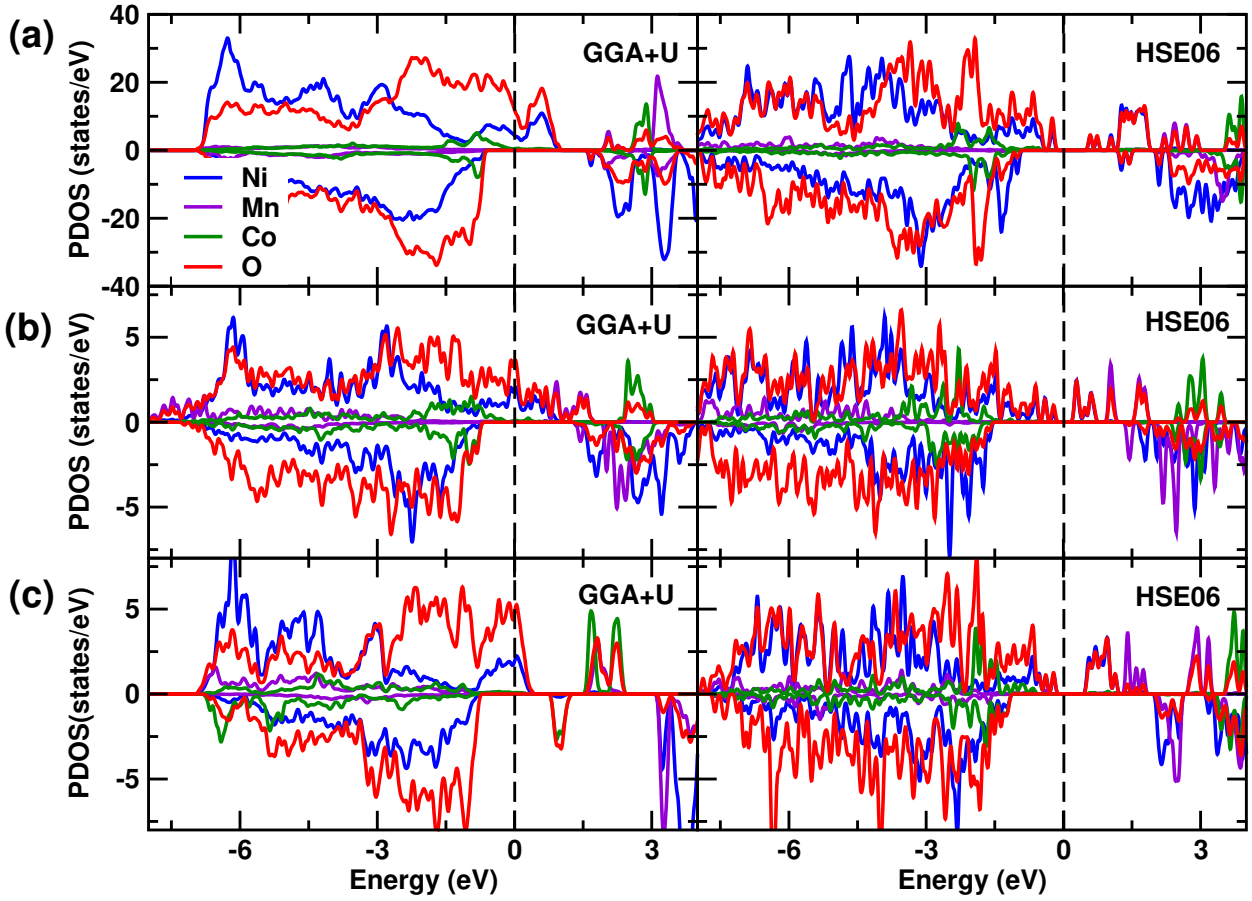

Figure 2: Density of states of NMC-811 and NMC-411. (a) left panel shows the GGA+U DOS for the NMC-811 rhombohedral structure, (b) left panel shows the same for NMC-411 rhombohedral structure, and (c) left panel shows the same for NMC-411 monoclinic structure, with the corresponding HSE06 DOS in the corresponding right panels. The bulk electronic structures are similar to each other at the same level of theory.

https://doi.org/10.26434/chemrxiv-2024-bjzbt **ORCID:** https://orcid.org/0000-0001-7852-497X Content not peer-reviewed by ChemRxiv. **License:** CC BY-NC-ND 4.0

0.5eV for the rhombohedral NMC-811, rhombohedral NMC-411, and monoclinic NMC-411 models, respectively. The HSE06 functional also provides a much better description of band renormalisation compared to GGA+U. GGA+U shifts TM d states to much lower energies compared to O p states since a Hubbard U correction is applied only to TM d and not to O p states. This causes a possibly unphysical representation of relative positions of TM d and O p states. The renormalisation due to HSE06 is applied to all states and is a more uniform renormalisation of bands in general. Moreover, HSE06 is a non-local functional and is more apt, particularly for describing non-local states like O p states. Thus, we conclude that calculations of observable properties should be performed at HSE or higher levels of theory; critically the theory used must include the self-interaction corrections that are missing in DFT.

Since all three structures show similar overall bulk electronic structure within the same level of theory (half metallic for PBE+U and insulating for HSE), we now use a smaller supercell as a proxy for the larger supercell. Specifically, NMC-411 is used as a proxy model for NMC-811, reproducing many of the electronic properties of NMC-811. Both stoichiometries are half-metallic in 0 K DFT+U calculations, and (correctly) insulating within HSE06 and have very similar band renormalisation at both levels of theory.

A further significant finding is that both the rhombohedral NMC-411 and the monoclinic NMC-411 have very similar bulk PDOS, indicating that the clustering (in rhombohedral) and de-clustering (in monoclinic) of dopants does not affect the overall average electronic behaviour of the bulk material, at the level of ground state 0K DFT. Thus, we have a reliable and consistent model for NMC which can be used in further more expensive calculations. Dopant clustering, nevertheless, can still have an impact on the local electronic structure of the material.

For completeness, we show in the SI the HSE06 DOS for NMC-321, 532, 611 (monoclinic) and 711, all of which are insulating/semiconducting at the level of HSE06. NMC-10-1-1 which contains about 83% Ni on the TM sites has an electronic structure that is similar

https://doi.org/10.26434/chemrxiv-2024-bjzbt **ORCID:** https://orcid.org/0000-0001-7852-497X Content not peer-reviewed by ChemRxiv. **License:** CC BY-NC-ND 4.0

to that of rhombohedral LNO: even HSE06 with 25% Fock exchange does not show an insulating state. However, up to 80% Ni can be satisfactorily described by HSE06. The degree of accuracy of the different levels of theory is, therefore, strongly dependent on the fraction of Ni in NMC. While higher values of Fock exchange may potentially result in an insulating state at high Ni contents, the results will likely be unphysical. However, the importance of non-local exchange is demonstrated clearly here: HSE06 does not include any self-interaction correction hence the treatment of correlation is at the level of single-particle PBE. Without resorting to expensive beyond DFT methods to include self-energy terms, we conclude that HSE is the most appropriate functional at the single-particle level to obtain the electronic structure of the Ni-rich NMCs. Although the usefulness of HSE06 functional has been discussed previously in terms of its accuracy in the prediction of redox potentials and charge transfer in LCO and LNO,[64] to the best of our knowledge an extensive study of NMCs with HSE06 functional is lacking.

We also wish to examine not just the 0 K magnetically ordered ground state as obtained from DFT but also the room temperature paramagnetic configurations, temperatures at which a real battery operates. DMFT calculations are ideally placed for examining such conditions. However multi-impurity DMFT calculations are extremely computationally expensive hence our NMC-411 simulation cells are ideally suited to carry out such calculations. In this case, for rhombohedral NMC-411 we end up with 6 impurities (4 Ni sites, 1 Mn site, 1 Co site) which is unwieldy. We solve this by treating each layer as strongly localised and independent of other layers. Hence, we solve in total three 2-impurity problems (Ni-Ni, Ni-Mn, Ni-Co) for each layer at the DMFT level, in a similar manner as done previously for LMO.[40] We shall use rhombohedral NMC-411 as our model system for the rest of our calculations of XANES spectra and for the DMFT-based determination of charges and correlated spectral functions.

https://doi.org/10.26434/chemrxiv-2024-bjzbt **ORCID:** https://orcid.org/0000-0001-7852-497X Content not peer-reviewed by ChemRxiv. **License:** CC BY-NC-ND 4.0

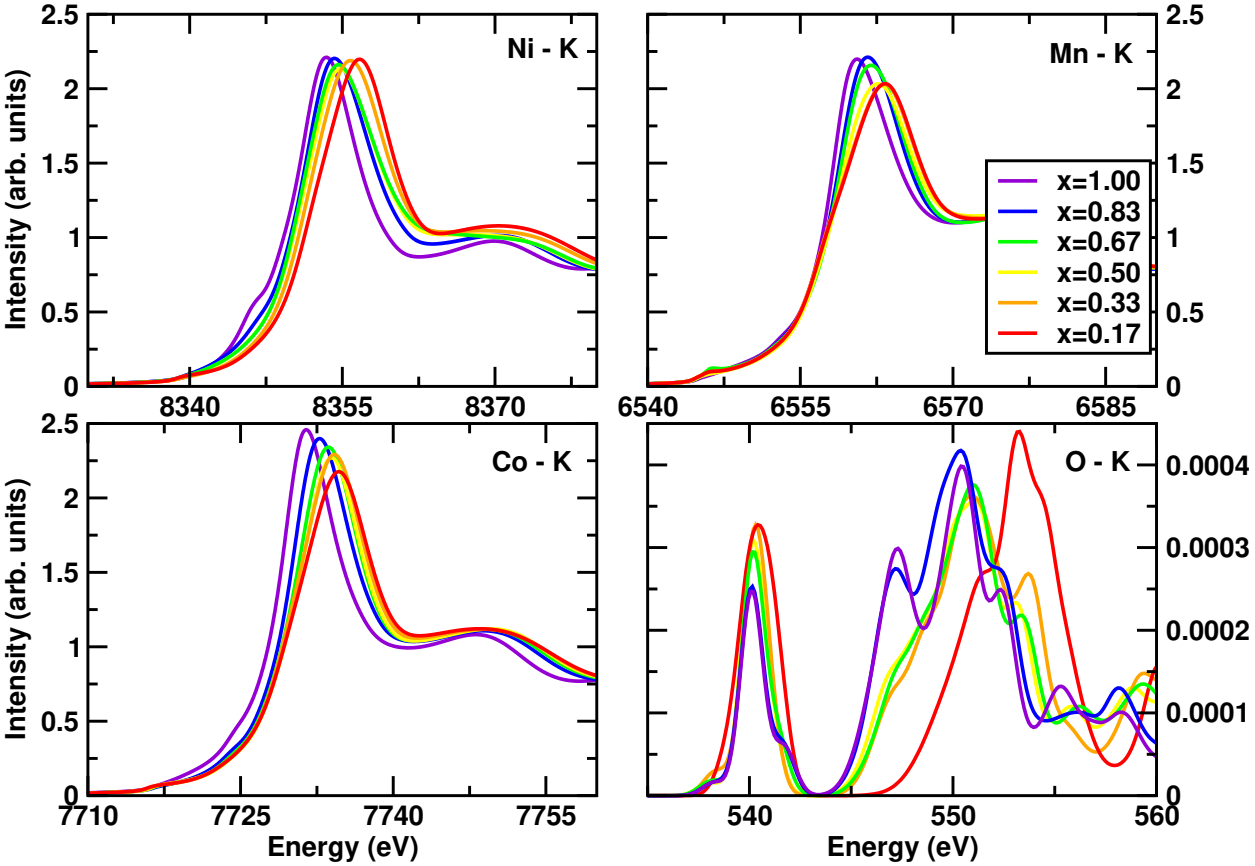

Figure 3: Calculated XANES spectra for transition metal K edges as a function of state-of-charge for Ni-rich NMCs. The theoretical spectra are calculated using an ab initio multiple scattering code (FEFF10). The calculated data shows an excellent match with the experimental spectra. Ni and Co K edges are seen to shift as a function of the state-of-charge, whereas the Mn K edge is seen to show a shift only in the higher intensity regime above half-maxima intensity (For experimental TM K edge data cf. Fig S6 and Fig S7 in SI by Kondrakov et al.[29] reused with permission from ACS.)

https://doi.org/10.26434/chemrxiv-2024-bjzbt **ORCID:** https://orcid.org/0000-0001-7852-497X Content not peer-reviewed by ChemRxiv. **License:** CC BY-NC-ND 4.0

Calculation of XANES spectra

Next, we explore the XANES spectra of both the TM and O K-edges. XANES is a powerful experimental tool for probing local structural environments, both in terms of oxidation states and bonding geometries. There is, however, no reliable way to deconvolute the effects of these two phenomena on the experimental spectra, *i.e.*, changes in the XANES K-edge could arise from changes in the oxidation state and/or changes in bond lengths, angles, *etc.*

To calculate the TM K edge in this work we employ the FEFF code, which previously gave us an excellent match between the calculated Ni K edge and the experimentally obtained Ni K edge from XANES experiments.[31] Our FEFF calculations incorporate a Green's function based self-energy within the GW_0 Approximation using the Hedin-Lundqvist plasmon-pole model. GW_0 includes effects of electron–electron interactions such as mean-free paths and self-energy shifts. FEFF calculations are usually a good approximation for EXAFS and reasonable for XANES.[65] However, GW_0 does not take into account spin fluctuations in the self-energy calculations. Moreover, in the GW_0 calculations, the inclusion of self-energy is itself at the level of a first-order approximation.[1]

We find from our FEFF calculations that the TM K-edge spectra of our rhombohedral NMC-411 unit cell shift upon delithiation in excellent agreement with experimentally obtained TM K edge spectra for NMC-811,[29] as shown in Fig. 3

The XANES K-edge is said to have *shifted* if there is a change in energy of the K-edge at the point of half of the maxima of the edge; this is the case for the Ni and Co but not the Mn K edges as a function of x or Li content. On the other hand, if there is no clear change in energy at this point however still there is a change in energy of the edge spectra near the maxima of the spectral intensity curve, this is known as *rotation* of the spectra[29]

There is a clear shift in the Ni and Co K edges, while the Mn K-edges do not shift but rather exhibit a rotation at the top of the K-edge spectra. The shift in Ni and Co K-edges has

[1]That is, the Taylor expansion of the self-energy, Σ, in terms of the single-particle Green's function, G, and the screened Coulomb interaction, W, is truncated after the first term $\Sigma \approx iGW$. Hence higher order effects are ignored.

https://doi.org/10.26434/chemrxiv-2024-bjzbt ORCID: https://orcid.org/0000-0001-7852-497X Content not peer-reviewed by ChemRxiv. License: CC BY-NC-ND 4.0

been attributed to TM oxidation, while the changes in the Mn K-edge have been attributed to changes in the local environment of Mn on delithation.[29,66,67] The experimental Co K-edge shows a shift to higher energy at the end of the charge, whereas in our calculations we observe a slightly higher shift at the beginning of the charge. This may either be due to Co (de-)clustering effects that our model is too small to capture or the missing spin fluctuations and higher-order effects as mentioned in the previous paragraph.

The observed edge shifts in both theoretical and experimental Ni and Co K edge XANES have been interpreted as indicating a change in oxidation state,[29] whereas the change in Mn K-edge is generally explained as a change in the local environment of the MnO_6 octahedra[29] Charges calculated by FEFF (although not very accurate) do not agree with the change in oxidation state as the only interpretation of the shift of XANES edge. Even though a clear shift of Ni K-edge is seen, FEFF charges, as shown in SI do not show the expected +1 change in formal oxidation state at each step as expected. Thus, we require a better method to calculate charges and oxidation states, ideally one taking into account both charge transfer due to covalency and strong-correlation effects, to be discussed in the next section.

Finally, we examine the O K-edge spectra. Unlike TMs, which are strongly correlated and require beyond DFT methods for proper inclusion of self energies, O is not regarded as a strongly correlated ion and hence core hole calculations at the level of HSE are sufficient to describe correctly O K-edge spectra. We find a very good match between HSE06 and experimental O K-edge spectra.

Firstly, HSE06 correctly reproduces the shoulder on the pre-edge peak at 541 eV (a peak not present in LNO O K-edge spectra).[67] The shoulder was assigned based on excited-state projected DOS calculations. A contribution to this shoulder comes from the split in the PDOS seen in the conduction bands due to the partially ordered magnetic state of Mn. The ordered magnetism in Mn survives up to a high temperature due to the higher T_C for Mn. The conduction band DOS is split in energy between up and down bands due to the strong ordered magnetism seen in Ni and Mn species in DFT. The shoulder vanishes on delithiation

https://doi.org/10.26434/chemrxiv-2024-bjzbt ORCID: https://orcid.org/0000-0001-7852-497X Content not peer-reviewed by ChemRxiv. License: CC BY-NC-ND 4.0

both in experiments[67] and in our calculated spectra. As the system is delithiated, a more correlated metallic phase appears, as we shall demonstrate in the next section using DMFT. A correlated metallic phase is one where the bandwidth of the band is comparable to Coulomb repulsion U. Unlike free electron metallicity which shows an almost parabolic dispersion and a delocalised band character, these states are prevalent in strongly correlated open d shell materials characterised by usually flatter bands and more localised states. This correlated metallic state reduces both the magnitude of moments and the ordering of moments. Hence now there is no such split in the empty bands in the excited-state DOS, leading to the vanishing of the shoulder-like feature. Hence the vanishing of the shoulder can actually be attributed to the emergence of correlated metallicity, which causes localised moments to become more delocalised and reduces the split in PDOS. The intensity of the pre-edge peak, which is usually[31,68] attributed to TM-O hybridisation, increases on delithiation in our HSE06 XAS calculations, as is also seen in experiments. While the edge itself has some small changes on delithiation, the overall change in the post-edge spectra on delithiation is much larger. The overall change in O K-edge indicates greater involvement of the O states in the redox process, through strong covalency with Ni centres.

Paramagnetic state: Charges and spectral functions from DMFT

Batteries are operated, and most degradation phenomena in cathodes are investigated experimentally, at or above room temperature, where NMC is in the paramagnetic phase.[13–15,68] These states are not accessible using conventional 0K DFT but can be described within DMFT, which yields correlated spectral functions at finite temperature (which can be thought of as the DMFT analogue of the DOS from DFT).

One of the main goals of this study is to assign the oxidation states correctly to different redox species in NMC. By integrating over the impurity Green's functions from DMFT the charges can be obtained at finite temperature. We do this first on NMC-111, which is the simplest system and easiest to benchmark with experimental systems. We next move

https://doi.org/10.26434/chemrxiv-2024-bjzbt ORCID: https://orcid.org/0000-0001-7852-497X Content not peer-reviewed by ChemRxiv. License: CC BY-NC-ND 4.0

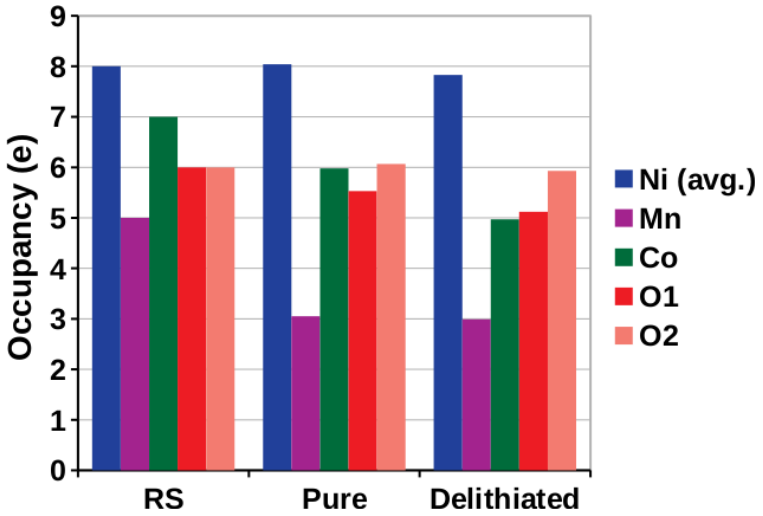

Figure 4: Calculated charges for the constructed RS, pristine and fully (100%) delithiated phase of rhombohedral NMC-411 model from DMFT calculations. Charges are calculated by integrating over the interacting Green's functions. Ni charges are seen to vary very little with charging and discharging. Co is seen to undergo oxidation on delithiation. Mn is in a d^3 state throughout. O shows a dual behaviour based on the combination of models for calculation. O in Ni-rich regions show redox behaviour however O in non-Ni-rich regions do not show redox behaviour. This also accounts for the relative stability of NMC systems compared to pristine LNO towards oxygen loss at high states of charge

on to the Ni-rich NMC phases. However, these are computationally expensive calculations hence we again use the smaller rhombohedral NMC-411 unit cell as a prototype for Ni-rich NMC phases in general. We carry out this analysis for the pristine NMC-411 model, 100% delithiated NMC-411 model, and the constructed prototype rock salt structural model of NMC (cf. SI for structure) as shown in Fig 4.

To construct the Wannier model for DMFT calculations on NMC-111, we examine the DFT band structure first (cf SI). We find no significant band overlap of the TM d and O p states hence we can employ Wannier d models and any hybridisation of TM d with O p will be considered in the contributions to the tails of the Wannier functions. We find that Ni is in a d^8 state, Mn is in a d^3 state and Co is in a d^6 state. Hence Ni is in a +2 oxidation state, Mn is in a +4 oxidation state, and Co is in a +3 oxidation state. This matches extremely well with previously obtained charges and oxidation states for NMC-111 and thus gives us a successful benchmarking of our method.[61,69]

https://doi.org/10.26434/chemrxiv-2024-bjzbt ORCID: https://orcid.org/0000-0001-7852-497X Content not peer-reviewed by ChemRxiv. License: CC BY-NC-ND 4.0

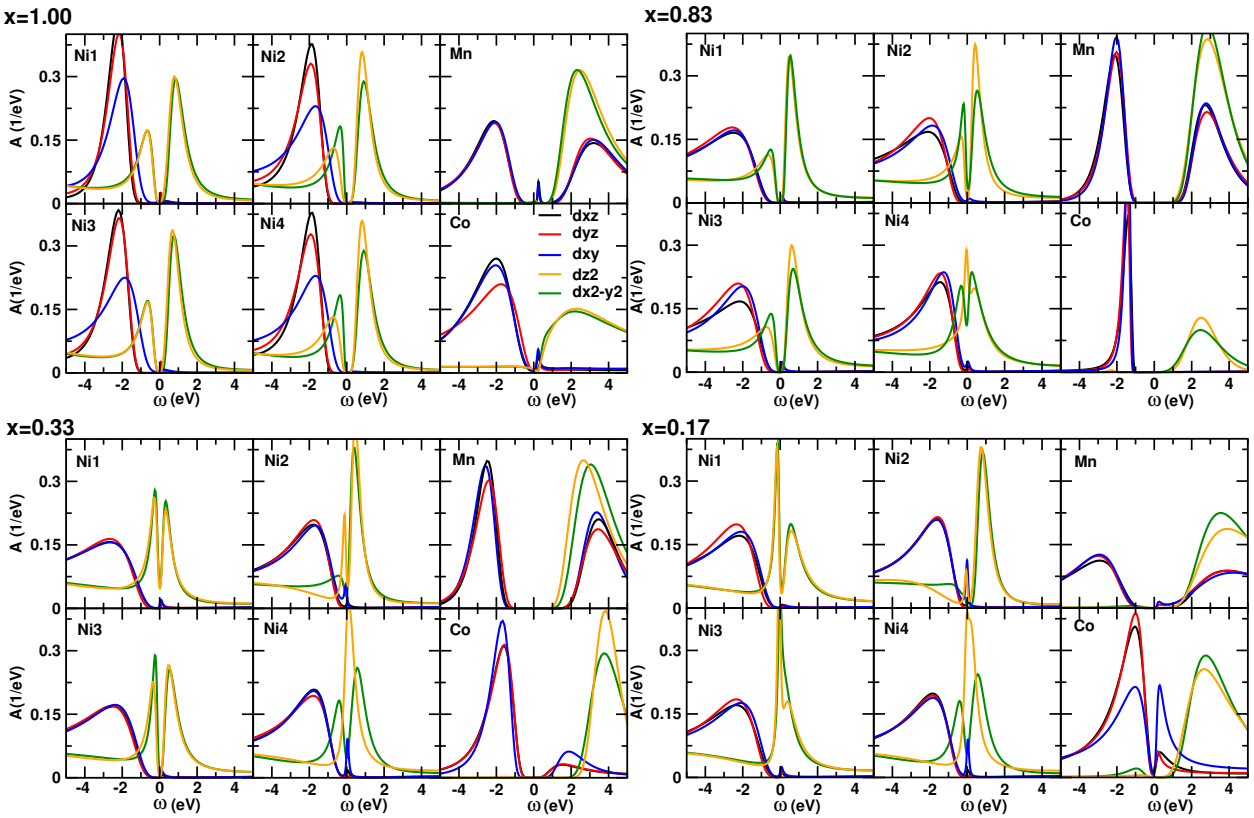

Figure 5: DMFT paramagnetic correlated spectral functions calculated at T=580K for pristine NMC-411 and at low and high states of charge. Spectral functions for all 4 Ni atoms, as well as Mn and Co atoms, are shown and resolved in terms of t_{2g} and e_g orbitals. For x=1 a semiconducting state with a small band gap and a quasiparticle behaviour is observed. A metal-insulator transition driven by quasiparticle interaction from pristine $X = 1$ to a delithiated state of $x = 0.83$ is seen. A strong quasiparticle peak is seen emerging for $x = 0.83$. A change in the Co oxidation state is seen to start at $x = 0.33$ contrary to previous DFT calculations.

https://doi.org/10.26434/chemrxiv-2024-bjzbt **ORCID:** https://orcid.org/0000-0001-7852-497X Content not peer-reviewed by ChemRxiv. **License:** CC BY-NC-ND 4.0

Next, we look at the DFT band structure of the rhombohedral NMC-411 structure to construct the Wannier models for our rhombohedral NMC-411 (as shown in the SI). We observe a large overlap between Ni d and O p bands, whereas there exists no explicit overlap between Mn d/Co d bands and O p bands. Hence, we construct a dp model for possible charge transfer effects in the Ni-O covalent system and a d-only model for Mn and Co. Our model is hence justified for each of the TM elements based on the comparison of DFT band structures shown in the SI.

Another important point here is the comparison between NMC-411 in rhombohedral and monoclinic structures. The DFT band structure of the monoclinic model, which contains isolated Mn and Co atoms, shows that the d electrons in these species are even more localised than that in the rhombohedral model. Hence with no clustering of Mn and Co and hence no Mn-O-Mn, and Co-O-Co superexchange paths a d model is sufficient. Usually a slightly higher than usual value of effective Hubbard U is required for better localisation as we have used here.

Charges obtained from our DMFT calculations show that in the case of the constructed RS structure Ni is in its "formal" oxidation state of +2. Hence Ni has an electron d-occupancy of d^8 and O has an occupancy of p^6 a similar result to NiO, the prototype RS. Next, we examine the charges for the other TM in the constructed RS phase. We see that Mn is in a d^5 state in a MnO configuration and Co is in a d^7 state and in a CoO configuration. This implies that all the O are in p^6 state. All the occupancies of the TM d and O p orbitals are shown in Fig. 4.

In the case of NMC-411, there are 4 Ni sites with very similar d orbital occupancies. Hence, we report the average occupancy for the pristine and delithiated structures for the sake of brevity. Ni on average has occupancies of d^8 and $d^{7.8}$ respectively.

Calculating O p occupancies gives us $p^{5.5}$ and $p^{5.1}$ respectively for the pristine and delithiated states. Hence these states correspond to classic $\mathrm{d}^8\underline{L}^1$ and $\mathrm{d}^8\mathrm{L}^2$ ligand-hole states with a large charge transfer from O p orbitals to Ni d orbitals and corresponding large ligand hole

https://doi.org/10.26434/chemrxiv-2024-bjzbt **ORCID:** https://orcid.org/0000-0001-7852-497X Content not peer-reviewed by ChemRxiv. **License:** CC BY-NC-ND 4.0

on O p orbitals surrounding Ni d orbitals. All the occupancies of the TM d and O p orbitals for the pristine and delithiated rhombohedral NMC-411 model are shown in Fig. 4.

Hence, we observe very little change in the charge state of Ni between the pristine, and delithiated cases. Similarly, as for LNO, the large charge transfer from O to Ni and the presence of ligand holes on the O indicate a greater involvement of O in the redox process in the Ni-rich regions as a part of a combined Ni-O covalent system.

We find Mn in a d^3 state and Co in a d^6 state in pristine rhombohedral NMC-411. Thus O here has p^6 occupancy for Mn-O-Mn/Ni and Co-O-Co/Ni superexchange paths, i.e. in non-Ni-rich regions. Significantly, this indicates that O has a dual behaviour within the materials, exhibiting charge states of p^6 and $p^{5.5}$ depending on its location. The O with $p^{5.5}$ occupied orbitals comprises the ligand hole state $\underline{L}^1$ from the Ni-O dp model.

Mn in the delithated rhombohedral NMC-411 model remains d^3 implying very little involvement in the redox process. In contrast Co changes oxidation state by 1 to d^5 on delithiation. O in this delithiated case remains p^6 by virtue of the use of the Wannier d model and the corresponding lack of charge transfer. Hence the charge imbalance on O is further enhanced by delithiation since now O shows the same dual behaviour as the pristine case albeit in states of p^6 and p^5 (with a larger ligand hole on O, $\underline{L}^2$ from the dp model of the Ni-O covalent system).

Thus, it is apparent from the calculated charges that the ideas of "formal" oxidation states and changes in "formal" oxidation states being correlated to shifts in TM XANES edges are not entirely coherent with the state-of-the-art methods of charge calculation and therefore the picture of ionic state changes requires some revision as a whole.

To track the redox process in the paramagnetic phase we next examine the correlated spectral functions obtained from DMFT at various states-of-charge, as shown in Fig. 5. First, we examine the spectral function for the pristine material at x=1.00. There are 4 Ni ions in the unit cell, however, we can see that Ni1 and Ni3 have very similar spectral functions and Ni2 and Ni4 also have similar spectral functions. Ni1 and Ni2 have spectral functions which

https://doi.org/10.26434/chemrxiv-2024-bjzbt **ORCID:** https://orcid.org/0000-0001-7852-497X Content not peer-reviewed by ChemRxiv. **License:** CC BY-NC-ND 4.0

differ very slightly due to different local environments. All 4 Ni are in Ni d^8L^1 ligand hole charge transfer states with filled t_{2g} and half-filled e_g orbitals and are semiconducting with a negligibly small gap at room temperature. We also see that Mn is in d^3 state with half-filled t_{2g} bands and empty e_g bands. Co is in a d^6 state with full t_{2g} bands and empty e_g bands. The band renormalisation here is much better than GGA+U and HSE06 functionals in each case. Hence we show again that even in the paramagnetic state of NMC, the conducting behaviour is not a half-metallic contrary to previous DFT studies using GGA/meta-GGA [28,30,32] but instead agrees with our HSE06 results wherein it is a vanishingly small gap semiconductor at finite temperatures. The agreement between HSE06 and DMFT matches well with previous experimental studies on the electronic conductivity of NMCs.

As the rhombohedral NMC-411 supercell is delithated, an insulator to correlated metal transition is driven at x=0.83 or 17% delithiation, with a large quasiparticle peak arising at the Ni4 site. This correlated metallic state does not represent free electron conductivity/metallicity but rather the presence of semi-localised quasiparticles represented by flat localised bands rather than dispersive parabolic bands of free electron metals, characterised by strongly interacting electronic states in the system.

Importantly even though we see a shift in e_g states of Ni, the charge state of Ni remains near the d^8L configuration and hence the full Ni-O covalent system participates in the redox process due to the strong Ni-O covalency. Like in LNO, this is contrary to the prevalent belief that Ni is the redox-active agent and O is merely a spectator in the process. [31] This in turn has a significant influence on the stability of the system as a whole due to the presence of the ligand holes on O, which makes the overall system unstable. At this state-of-charge, Mn and Co show very similar spectral functions as in the x=1.00 state and hence can be assumed to have not participated in the redox process yet.

Of particular interest to us are higher states of charge where the majority of the degradation phenomena take place. To this end, we examine the spectral functions at x=0.33 or a 67% state of delithiation. We see the emergence of quasiparticle peaks and hence correlated

https://doi.org/10.26434/chemrxiv-2024-bjzbt **ORCID:** https://orcid.org/0000-0001-7852-497X Content not peer-reviewed by ChemRxiv. **License:** CC BY-NC-ND 4.0

metallic states at both Ni2 and Ni4 sites which is a clear indication of the quasiparticle hopping, as shown in Fig. 5. Importantly we also see a change in the spectral functions of Co d states, showing the involvement of Co in the redox process at 67% state-of-charge. This is contrary to previous DFT studies[28] which observed that Co only got oxidised only at the very end of charge when they extract all the Li from the system. This may be due to the lack of self-interaction corrections within DFT which does not take into account the variation of quasiparticle weights due to correlation effects and hence consequently any interaction between electrons.

Finally at a very high state-of-charge at x=0.17 or 83% delithiated state, we see large quasiparticle peaks on Ni3 and Ni4 sites and small quasiparticle peaks on Ni2, confirming our idea of quasiparticle hopping. At the same time, Ni is in the d^8L^2 state confirming the idea of Ni-O covalent system participating in redox as a whole. Interestingly these quasiparticles may have limited mobility and affect both ionic and electronic conductivity of the system. It is also to be noted that the electronic conductivity depends on the quasiparticle weight, which is given by the spectral weight of the quasiparticle peak, which we do not go into here for the sake of brevity.

Discussion

Our calculations show that for NMC, like LNO, assigning changes in oxidation states to shifts in TM XANES spectra does not work as a standalone method to describe systems that are strongly covalent. These must be augmented by charge calculations and correlated spectral functions to accurately uncover redox behaviour. In NMC, our observation of Ni charges showing little to no change on delithiation implies a greater involvement of O in the redox process, however, combined with the changes in Ni d correlated spectral functions and the emergence of quasiparticle peak, we conclude that the Ni-O complex as a whole takes part in the redox process, with Ni in a d^8L ligand hole charge transfer state. Hence particularly

https://doi.org/10.26434/chemrxiv-2024-bjzbt **ORCID:** https://orcid.org/0000-0001-7852-497X Content not peer-reviewed by ChemRxiv. **License:** CC BY-NC-ND 4.0

in Ni-rich regions for Ni-O-Ni superexchange paths in NMC cathodes, O p orbitals have a much stronger involvement in redox processes and as a consequence of the ligand hole on the O p states, the stability of the cathode is majorly influenced.

Our model allows us to study Ni-rich regions separately from regions where dopants are situated next to Ni. From the DMFT charges we show the dual behaviour of O redox. We observe that in the Ni-rich regions, with Ni-O-Ni superexchange paths, O is more involved in the redox process through the Ni-O covalent system and has a significant change of charge states due to large covalency with Ni. In the regions where Ni-O-Ni superexchange paths are replaced with Ni-O-Co superexchange paths, there is very little involvement of O in the redox process, and Co is majorly involved in the redox. This indicates for Ni-O-Co superexchange paths the effect of ligand hole formation on O is much reduced. For the cases of Ni-O-Mn, there is little redox activity, other than the small change in the redox behaviour of the Ni-O covalent system. An increase in Ni content causes more and more O to have ligand holes in the vicinity of the Ni-rich regions, in the Ni-O-Ni superexchange paths. This explains clearly why lower Ni content NMCs have higher stability and higher Ni content NMCs have lower stability and LNO, the extreme case comprising 100% Ni, has the least stability.

The question of stability also brings us to briefly consider methods to mitigate issues like O loss and singlet O generation. We show that Co starts to participate at a state-of-charge of x=0.33 in the redox process. The dual behaviour of O is seen with ligand holes on some sites in Ni-rich regions and no ligand holes in non-Ni-rich regions. Previous studies of LNO have shown O at the surface to be even more unstable than at the bulk.[31] Coating Ni-rich NMC/LNO with standard coating materials like Al_2O_3[70] or LCO hence might be a very effective method to suppress O loss and singlet O generation due to the reduction of O ligand holes on Ni-rich surfaces. Using LCO as a coating on NMC core also improves electrochemical activity over Al_2O_3 coating, which is not a cathode-active material. Surface O species are even more unstable due to surface effects and dangling O bonds which are well known in oxide literature.[71] Hence coating NMC or other Ni-rich cathode materials

https://doi.org/10.26434/chemrxiv-2024-bjzbt **ORCID:** https://orcid.org/0000-0001-7852-497X Content not peer-reviewed by ChemRxiv. **License:** CC BY-NC-ND 4.0

with more stable cathode active materials like LCO can be a possible answer towards higher stability of Ni-rich cathode materials.

Conclusion

Employing many-body physics methods in conjunction with theoretical spectroscopic methods we studied the redox behavior in Ni-rich NMC cathodes as a function of (de)lithiation. Our calculations show an excellent match of calculated Ni, Mn, and Co K-edges as a function of the state-of-charge with experimentally obtained XANES spectra. Our study reveals that contrary to the ionic picture of cathode redox, Ni remains in a $d^8\underline{\mathrm{L}}$ ligand hole charge transfer state throughout the charging/discharging process, particularly in Ni-rich environments due to strong Ni-O covalency and that the Ni-O covalent system shows redox behavior as a whole. Additionally, we demonstrate that O has dual redox behavior and shows greater involvement in redox in Ni-rich regions (Ni-O-Ni superexchange paths) due to strong Ni-O covalency while staying at its formal oxidation state of -2 in Ni-poor regions (Ni-O-Mn/Co superexchange paths). We also illustrate a strong electron-electron interaction driven insulator to correlated metal transition accompanied by the emergence of quasiparticle peaks due to these strong electron-electron interactions as a function of the state-of-charge. Contrary to previous DFT results, we clarify that Co oxidation does not occur with the extraction of the last Li ion, but rather at an earlier state-of-charge at x=0.33, whereas the Ni-O system starts participating around a state-of-charge at x=0.83, which is the beginning of charge in our system.

We hence demonstrate that the ionic model of describing changes in metal oxidation states as a function of shift in XANES edges is insufficient in NMCs, particularly in cases of strong transition metal and oxygen covalency, and state-of-the-art methods of calculating correlated spectral functions and charge analysis based on interacting Green's functions are required to be used along with XANES spectra to determine redox behaviour in complex

https://doi.org/10.26434/chemrxiv-2024-bjzbt **ORCID:** https://orcid.org/0000-0001-7852-497X Content not peer-reviewed by ChemRxiv. **License:** CC BY-NC-ND 4.0

cathode materials. Finally, our study sheds light on why NMCs are more stable in terms of cathode degradation compared to LNO and the relative higher stability of lower Ni content NMCs.

Acknowledgements

The authors acknowledge fruitful discussions with Louis Piper, Robert Weatherup, Ieuan Seymour, Annalena R. Genreith-Schriever, and Junpei Shi. This work was supported by the Faraday Institution (FIRG024, FIRG060). Calculations have been performed on the Odyssey cluster, the CSD3 cluster of the University of Cambridge, the Brookhaven National Lab HPC supercomputer (access provided through the centre for functional nanomaterials), the Sulis Supercomputing Cluster of HPC Midlands+, Archer2 (access provided through the Materials Chemistry Consortium), and Michael HPC supercomputing cluster of University College London (access provided through the Faraday Institution degradation project). Generous computing resources were provided by MCC on Archer2, Sulis HPC service (EP/T022108/1), and networking support by CCP-NC (EP/T026642/1), CCP9 (EP/T026375/1), and UKCP (EP/P022561/1).

References

(1) Mizushima, K.; Jones, P.; Wiseman, P.; Goodenough, J. Li_xCoO_2 (0<x<1): A new cathode material for batteries of high energy density. *Materials Research Bulletin* **1980**, *15*, 783–789.

(2) Thackeray, M.; David, W.; Bruce, P.; Goodenough, J. Lithium insertion into manganese spinels. *Materials Research Bulletin* **1983**, *18*, 461–472.

(3) Liu, Z.; Yu, A.; Lee, J. Y. Synthesis and characterization of LiNi1-x-yCoxMnyO2 as

https://doi.org/10.26434/chemrxiv-2024-bjzbt **ORCID:** https://orcid.org/0000-0001-7852-497X Content not peer-reviewed by ChemRxiv. **License:** CC BY-NC-ND 4.0

the cathode materials of secondary lithium batteries. *Journal of Power Sources* **1999**, *81-82*, 416–419.

(4) Tarascon, J.-M.; Armand, M. Issues and challenges facing rechargeable lithium batteries. *Nature* **2001**, *414*, 359–367.

(5) Ohzuku, T.; Makimura, Y. Layered Lithium Insertion Material of LiCo1/3Ni1/3Mn1/3O2 for Lithium-Ion Batteries. *Chemistry Letters* **2003**, *30*, 642–643.

(6) Wang, G.; Bewlay, S.; Yao, J.; Chen, Y.; Guo, Z.; Liu, H.; Dou, S. Multiple-ion-doped lithium nickel oxides as cathode materials for lithium-ion batteries. *Journal of Power Sources* **2003**, *119-121*, 189–194, Selected papers presented at the 11th International Meeting on Lithium Batteries.

(7) Kim, M.-H.; Shin, H.-S.; Shin, D.; Sun, Y.-K. Synthesis and electrochemical properties of Li[Ni0.8Co0.1Mn0.1]O2 and Li[Ni0.8Co0.2]O2 via co-precipitation. *Journal of Power Sources* **2006**, *159*, 1328–1333.

(8) Choi, J.; Manthiram, A. Crystal chemistry and electrochemical characterization of layered $LiNi_{0.5y}Co_{0.5y}Mn_{2y}O_2$ and $LiCo_{0.5y}Mn_{0.5y}Ni_{2y}O_2$ (0<2y<1) cathodes. *Journal of Power Sources* **2006**, *162*, 667–672.

(9) Chernova, N. A.; Ma, M.; Xiao, J.; Whittingham, M. S.; Breger, J.; Grey, C. P. Layered LixNiyMnyCo1-2yO2 Cathodes for Lithium Ion Batteries: Understanding Local Structure via Magnetic Properties. *Chemistry of Materials* **2007**, *19*, 4682–4693.

(10) Wu, Z.; Ji, S.; Zheng, J.; Hu, Z.; Xiao, S.; Wei, Y.; Zhuo, Z.; Lin, Y.; Yang, W.; Xu, K.; Amine, K.; Pan, F. Prelithiation Activates Li(Ni0.5Mn0.3Co0.2)O2 for High Capacity and Excellent Cycling Stability. *Nano Letters* **2015**, *15*, 5590–5596.

https://doi.org/10.26434/chemrxiv-2024-bjzbt **ORCID:** https://orcid.org/0000-0001-7852-497X Content not peer-reviewed by ChemRxiv. **License:** CC BY-NC-ND 4.0

(11) Blomgren, G. E. The Development and Future of Lithium Ion Batteries. *Journal of The Electrochemical Society* **2016**, *164*, A5019.

(12) Li, W.; Erickson, E. M.; Manthiram, A. High-nickel layered oxide cathodes for lithium-based automotive batteries. *Nature Energy* **2020**, *5*, 26–34.

(13) Märker, K.; Reeves, P. J.; Xu, C.; Griffith, K. J.; Grey, C. P. Evolution of Structure and Lithium Dynamics in LiNi0.8Mn0.1Co0.1O2 (NMC811) Cathodes during Electrochemical Cycling. *Chemistry of Materials* **2019**, *31*, 2545–2554.

(14) Märker, K.; Xu, C.; Grey, C. P. Operando NMR of NMC811/Graphite Lithium-Ion Batteries: Structure, Dynamics, and Lithium Metal Deposition. *Journal of the American Chemical Society* **2020**, *142*, 17447–17456.

(15) Ruff, Z.; Coates, C. S.; Märker, K.; Mahadevegowda, A.; Xu, C.; Penrod, M. E.; Ducati, C.; Grey, C. P. O3 to O1 Phase Transitions in Highly Delithiated NMC811 at Elevated Temperatures. *Chemistry of Materials* **2023**, *35*, 4979–4987.

(16) Manthiram, A.; Song, B.; Li, W. A perspective on nickel-rich layered oxide cathodes for lithium-ion batteries. *Energy Storage Materials* **2017**, *6*, 125–139.

(17) Noh, H.-J.; Youn, S.; Yoon, C. S.; Sun, Y.-K. Comparison of the structural and electrochemical properties of layered Li[NixCoyMnz]O2 (x = 1/3, 0.5, 0.6, 0.7, 0.8 and 0.85) cathode material for lithium-ion batteries. *Journal of Power Sources* **2013**, *233*, 121–130.

(18) Zeng, D.; Cabana, J.; Bréger, J.; Yoon, W.-S.; Grey, C. P. Cation Ordering in Li[NixMnxCo(1–2x)]O2-Layered Cathode Materials: A Nuclear Magnetic Resonance (NMR), Pair Distribution Function, X-ray Absorption Spectroscopy, and Electrochemical Study. *Chemistry of Materials* **2007**, *19*, 6277–6289.

https://doi.org/10.26434/chemrxiv-2024-bjzbt **ORCID:** https://orcid.org/0000-0001-7852-497X Content not peer-reviewed by ChemRxiv. **License:** CC BY-NC-ND 4.0

(19) Bak, S.-M.; Hu, E.; Zhou, Y.; Yu, X.; Senanayake, S. D.; Cho, S.-J.; Kim, K.-B.; Chung, K. Y.; Yang, X.-Q.; Nam, K.-W. Structural Changes and Thermal Stability of Charged LiNixMnyCozO2 Cathode Materials Studied by Combined In Situ Time-Resolved XRD and Mass Spectroscopy. *ACS Applied Materials & Interfaces* **2014**, *6*, 22594–22601.

(20) Nam, K.-W.; Bak, S.-M.; Hu, E.; Yu, X.; Zhou, Y.; Wang, X.; Wu, L.; Zhu, Y.; Chung, K.-Y.; Yang, X.-Q. Combining In Situ Synchrotron X-Ray Diffraction and Absorption Techniques with Transmission Electron Microscopy to Study the Origin of Thermal Instability in Overcharged Cathode Materials for Lithium-Ion Batteries. *Advanced Functional Materials* **2013**, *23*, 1047–1063.

(21) Wood, M.; Sheng, Y.; Keever, T. J.; Li, J.; Wood, D. L. Stability of Ni-Rich NMC Cathode Materials in Water and Electrolyte Solutions during Aqueous Electrode Processing. *ECS Meeting Abstracts* **2017**, *MA2017-01*, 376.

(22) Jung, R.; Metzger, M.; Maglia, F.; Stinner, C.; Gasteiger, H. A. Oxygen Release and Its Effect on the Cycling Stability of LiNixMnyCozO2 (NMC) Cathode Materials for Li-Ion Batteries. *Journal of The Electrochemical Society* **2017**, *164*, A1361.

(23) Dong, X.; Yao, J.; Zhu, W.; Huang, X.; Kuai, X.; Tang, J.; Li, X.; Dai, S.; Shen, L.; Yang, R.; Gao, L.; Zhao, J. Enhanced high-voltage cycling stability of Ni-rich cathode materials via the self-assembly of Mn-rich shells. *J. Mater. Chem. A* **2019**, *7*, 20262–20273.

(24) Lipson, A. L.; Durham, J. L.; LeResche, M.; Abu-Baker, I.; Murphy, M. J.; Fister, T. T.; Wang, L.; Zhou, F.; Liu, L.; Kim, K.; Johnson, D. Improving the Thermal Stability of NMC 622 Li-Ion Battery Cathodes through Doping During Coprecipitation. *ACS Applied Materials & Interfaces* **2020**, *12*, 18512–18518.

(25) Wood, M.; Li, J.; Ruther, R. E.; Du, Z.; Self, E. C.; Meyer, H. M.; Daniel, C.; Bel-

https://doi.org/10.26434/chemrxiv-2024-bjzbt **ORCID:** https://orcid.org/0000-0001-7852-497X Content not peer-reviewed by ChemRxiv. **License:** CC BY-NC-ND 4.0

harouak, I.; Wood, D. L. Chemical stability and long-term cell performance of low-cobalt, Ni-Rich cathodes prepared by aqueous processing for high-energy Li-Ion batteries. *Energy Storage Materials* **2020**, *24*, 188–197.

(26) Dose, W. M.; Temprano, I.; Allen, J. P.; Björklund, E.; O'Keefe, C. A.; Li, W.; Mehdi, B. L.; Weatherup, R. S.; De Volder, M. F. L.; Grey, C. P. Electrolyte Reactivity at the Charged Ni-Rich Cathode Interface and Degradation in Li-Ion Batteries. *ACS Applied Materials & Interfaces* **2022**, *14*, 13206–13222.

(27) Hou, D.; Xu, Z.; Yang, Z.; Kuai, C.; Du, Z.; Sun, C.-J.; Ren, Y.; Liu, J.; Xiao, X.; Lin, F. Effect of the grain arrangements on the thermal stability of polycrystalline nickel-rich lithium-based battery cathodes. *Nature Communications* **2022**, *13*, 3437.

(28) Dixit, M.; Markovsky, B.; Schipper, F.; Aurbach, D.; Major, D. T. Origin of Structural Degradation During Cycling and Low Thermal Stability of Ni-Rich Layered Transition Metal-Based Electrode Materials. *The Journal of Physical Chemistry C* **2017**, *121*, 22628–22636.

(29) Kondrakov, A. O.; Geßwein, H.; Galdina, K.; de Biasi, L.; Meded, V.; Filatova, E. O.; Schumacher, G.; Wenzel, W.; Hartmann, P.; Brezesinski, T.; Janek, J. Charge-Transfer-Induced Lattice Collapse in Ni-Rich NCM Cathode Materials during Delithiation. *The Journal of Physical Chemistry C* **2017**, *121*, 24381–24388.

(30) Sun, H.; Zhao, K. Electronic Structure and Comparative Properties of LiNixMnyCozO2 Cathode Materials. *The Journal of Physical Chemistry C* **2017**, *121*, 6002–6010.

(31) Genreith-Schriever, A. R.; Banerjee, H.; Menon, A. S.; Bassey, E. N.; Piper, L. F.; Grey, C. P.; Morris, A. J. Oxygen hole formation controls stability in $LiNiO_2$ cathodes. *Joule* **2023**, *7*, 1623–1640.

(32) Chakraborty, A.; Kunnikuruvan, S.; Kumar, S.; Markovsky, B.; Aurbach, D.; Dixit, M.; Major, D. T. Layered Cathode Materials for Lithium-Ion Batteries: Review of Com-

https://doi.org/10.26434/chemrxiv-2024-bjzbt **ORCID:** https://orcid.org/0000-0001-7852-497X Content not peer-reviewed by ChemRxiv. **License:** CC BY-NC-ND 4.0

putational Studies on LiNi1–x–yCoxMnyO2 and LiNi1–x–yCoxAlyO2. *Chemistry of Materials* **2020**, *32*, 915–952.

(33) Wang, S.; Yan, M.; Li, Y.; Vinado, C.; Yang, J. Separating electronic and ionic conductivity in mix-conducting layered lithium transition-metal oxides. *Journal of Power Sources* **2018**, *393*, 75–82.

(34) Mukherjee, P.; Paddison, J. A. M.; Xu, C.; Ruff, Z.; Wildes, A. R.; Keen, D. A.; Smith, R. I.; Grey, C. P.; Dutton, S. E. Sample Dependence of Magnetism in the Next-Generation Cathode Material LiNi0.8Mn0.1Co0.1O2. *Inorganic Chemistry* **2021**, *60*, 263–271.

(35) Wikberg, J. M.; Dahbi, M.; Saadoune, I.; Gustafsson, T.; Edstrom, K.; Svedlindh, P. Magnetic order, aging, and spin frustration in a percolating spin system, LiNi0.8Co0.1Mn0.1O2. *Journal of Applied Physics* **2010**, *108*, 083909.

(36) Banerjee, H.; Aichhorn, M. Emergence of a ferromagnetic insulating state in $LaMnO_3/SrTiO_3$ heterostructures: Role of strong electronic correlations and strain. *Phys. Rev. B* **2020**, *101*, 241112.

(37) Banerjee, H.; Schnait, H.; Aichhorn, M.; Saha-Dasgupta, T. Effect of geometry on magnetism of Hund's metals: Case study of $BaRuO_3$. *Phys. Rev. B* **2022**, *105*, 235106.

(38) Yamasaki, A.; Feldbacher, M.; Yang, Y.-F.; Andersen, O. K.; Held, K. Pressure-Induced Metal-Insulator Transition in $LaMnO_3$ Is Not of Mott-Hubbard Type. *Phys. Rev. Lett.* **2006**, *96*, 166401.

(39) Yang, Y.-F.; Held, K. Localization of strongly correlated electrons as Jahn-Teller polarons in manganites. *Phys. Rev. B* **2007**, *76*, 212401.

(40) Banerjee, H.; Grey, C. P.; Morris, A. J. Importance of electronic correlations in exploring the exotic phase diagram of layered Li_xMnO_2. *Phys. Rev. B* **2023**, *108*, 165124.

https://doi.org/10.26434/chemrxiv-2024-bjzbt **ORCID:** https://orcid.org/0000-0001-7852-497X Content not peer-reviewed by ChemRxiv. **License:** CC BY-NC-ND 4.0

(41) Isaacs, E. B.; Marianetti, C. A. Compositional phase stability of correlated electron materials within DFT+DMFT. *Phys. Rev. B* **2020**, *102*, 045146.

(42) Blöchl, P. E. Projector augmented-wave method. *Phys. Rev. B* **1994**, *50*, 17953–17979.

(43) Kresse, G.; Hafner, J. Ab initio molecular dynamics for liquid metals. *Phys. Rev. B* **1993**, *47*, 558–561.

(44) Kresse, G.; Furthmüller, J. Efficient iterative schemes for ab initio total-energy calculations using a plane-wave basis set. *Phys. Rev. B* **1996**, *54*, 11169–11186.

(45) Blaha, P.; Schwarz, K.; Tran, F.; Laskowski, R.; Madsen, G. K. H.; Marks, L. D. WIEN2k: An APW+lo program for calculating the properties of solids. *The Journal of Chemical Physics* **2020**, *152*, 074101.

(46) Perdew, J. P.; Burke, K.; Ernzerhof, M. Generalized Gradient Approximation Made Simple. *Phys. Rev. Lett.* **1996**, *77*, 3865–3868.

(47) de Groot, F. Multiplet effects in X-ray spectroscopy. *Coordination Chemistry Reviews* **2005**, *249*, 31–63, Synchrotron Radiation in Inorganic and Bioinorganic Chemistry.

(48) Rehr, J. J.; Kas, J. J.; Vila, F. D.; Prange, M. P.; Jorissen, K. Parameter-free calculations of X-ray spectra with FEFF9. *Phys. Chem. Chem. Phys.* **2010**, *12*, 5503–5513.

(49) Kas, J. J.; Vila, F. D.; Pemmaraju, C. D.; Tan, T. S.; Rehr, J. J. Advanced calculations of X-ray spectroscopies with *FEFF10* and Corvus. *Journal of Synchrotron Radiation* **2021**, *28*, 1801–1810.

(50) Rehr, J. J.; Albers, R. C. Theoretical approaches to x-ray absorption fine structure. *Rev. Mod. Phys.* **2000**, *72*, 621–654.

(51) Aichhorn, M.; Pourovskii, L.; Vildosola, V.; Ferrero, M.; Parcollet, O.; Miyake, T.; Georges, A.; Biermann, S. Dynamical mean-field theory within an augmented plane-

https://doi.org/10.26434/chemrxiv-2024-bjzbt **ORCID:** https://orcid.org/0000-0001-7852-497X Content not peer-reviewed by ChemRxiv. **License:** CC BY-NC-ND 4.0

wave framework: Assessing electronic correlations in the iron pnictide LaFeAsO. *Phys. Rev. B* **2009**, *80*, 085101.

(52) Aichhorn, M.; Pourovskii, L.; Georges, A. Importance of electronic correlations for structural and magnetic properties of the iron pnictide superconductor LaFeAsO. *Phys. Rev. B* **2011**, *84*, 054529.

(53) Aichhorn, M.; Pourovskii, L.; Seth, P.; Vildosola, V.; Zingl, M.; Peil, O. E.; Deng, X.; Mravlje, J.; Kraberger, G. J.; Martins, C.; Ferrero, M.; Parcollet, O. TRIQS/DFTTools: A TRIQS application for ab initio calculations of correlated materials. *Computer Physics Communications* **2016**, *204*, 200 – 208.

(54) Parcollet, O.; Ferrero, M.; Ayral, T.; Hafermann, H.; Krivenko, I.; Messio, L.; Seth, P. TRIQS: A toolbox for research on interacting quantum systems. *Computer Physics Communications* **2015**, *196*, 398 – 415.

(55) Pizzi, G. et al. Wannier90 as a community code: new features and applications. *Journal of Physics: Condensed Matter* **2020**, *32*, 165902.

(56) Kuneš, J.; Arita, R.; Wissgott, P.; Toschi, A.; Ikeda, H.; Held, K. Wien2wannier: From linearized augmented plane waves to maximally localized Wannier functions. *Computer Physics Communications* **2010**, *181*, 1888–1895.

(57) Werner, P.; Millis, A. J. Hybridization expansion impurity solver: General formulation and application to Kondo lattice and two-orbital models. *Phys. Rev. B* **2006**, *74*, 155107.

(58) Seth, P.; Krivenko, I.; Ferrero, M.; Parcollet, O. TRIQS/CTHYB: A continuous-time quantum Monte Carlo hybridisation expansion solver for quantum impurity problems. *Computer Physics Communications* **2016**, *200*, 274 – 284.

(59) Held, K. *Advances in Physics* **2007**, *56*, 829–926.

https://doi.org/10.26434/chemrxiv-2024-bjzbt **ORCID:** https://orcid.org/0000-0001-7852-497X Content not peer-reviewed by ChemRxiv. **License:** CC BY-NC-ND 4.0

(60) Kraberger, G. J.; Triebl, R.; Zingl, M.; Aichhorn, M. Maximum entropy formalism for the analytic continuation of matrix-valued Green's functions. *Phys. Rev. B* **2017**, *96*, 155128.

(61) Yoon, W.-S.; Balasubramanian, M.; Chung, K. Y.; Yang, X.-Q.; McBreen, J.; Grey, C. P.; Fischer, D. A. Investigation of the Charge Compensation Mechanism on the Electrochemically Li-Ion Deintercalated $Li_{1-x}Co_{1/3}Ni_{1/3}Mn_{1/3}O_2$ Electrode System by Combination of Soft and Hard X-ray Absorption Spectroscopy. *Journal of the American Chemical Society* **2005**, *127*, 17479–17487.

(62) Perdew, J. P.; Ruzsinszky, A.; Csonka, G. I.; Vydrov, O. A.; Scuseria, G. E.; Constantin, L. A.; Zhou, X.; Burke, K. Restoring the Density-Gradient Expansion for Exchange in Solids and Surfaces. *Phys. Rev. Lett.* **2008**, *100*, 136406.

(63) Zhang, G.-X.; Reilly, A. M.; Tkatchenko, A.; Scheffler, M. Performance of various density-functional approximations for cohesive properties of 64 bulk solids. *New Journal of Physics* **2018**, *20*, 063020.

(64) Seo, D.-H.; Urban, A.; Ceder, G. Calibrating transition-metal energy levels and oxygen bands in first-principles calculations: Accurate prediction of redox potentials and charge transfer in lithium transition-metal oxides. *Phys. Rev. B* **2015**, *92*, 115118.

(65) Mathew, K.; Zheng, C.; Winston, D.; Chen, C.; Dozier, A.; Rehr, J. J.; Ong, S. P.; Persson, K. A. High-throughput computational X-ray absorption spectroscopy. *Sci Data* **2018**, *5*, 180151.

(66) Alvarado, J.; Wei, C.; Nordlund, D.; Kroll, T.; Sokaras, D.; Tian, Y.; Liu, Y.; Doeff, M. M. Thermal stress-induced charge and structure heterogeneity in emerging cathode materials. *Materials Today* **2020**, *35*, 87–98.

(67) Kleiner, K.; Murray, C. A.; Grosu, C.; Ying, B.; Winter, M.; Nagel, P.; Schup-

https://doi.org/10.26434/chemrxiv-2024-bjzbt **ORCID:** https://orcid.org/0000-0001-7852-497X Content not peer-reviewed by ChemRxiv. **License:** CC BY-NC-ND 4.0

pler, S.; Merz, M. On the Origin of Reversible and Irreversible Reactions in LiNixCo(1-x)/2Mn(1-x)/2O2. *Journal of The Electrochemical Society* **2021**, *168*, 120533.

(68) Menon, A. et al. Oxygen-Redox Activity in Non-Lithium-Excess Tungsten-Doped $LiNiO_2$ Cathode. *PRX Energy* **2023**, *2*, 013005.

(69) Yoon, W.-S.; Grey, C. P.; Balasubramanian, M.; Yang, X.-Q.; Fischer, D. A.; McBreen, J. Combined NMR and XAS Study on Local Environments and Electronic Structures of Electrochemically Li-Ion Deintercalated Li_{1x} $Co_{1/3}Ni_{1/3}Mn_{1/3}O_2$ Electrode System. *Electrochemical and Solid-State Letters* **2004**, *7*, A53.

(70) Riesgo-González, V.; Hall, D. S.; Märker, K.; Slaughter, J.; Wright, D. S.; Grey, C. P. Effect of Annealing on the Structure, Composition, and Electrochemistry of NMC811 Coated with Al2O3 Using an Alkoxide Precursor. *Chemistry of Materials* **2022**, *34*, 9722–9735.

(71) Yasumura, S.; Kamachi, T.; Toyao, T.; Shimizu, K.-i.; Hinuma, Y. Prediction of Stable Surfaces of Metal Oxides through the Unsaturated Coordination Index. *ACS Omega* **2023**, *8*, 29779–29788.

https://doi.org/10.26434/chemrxiv-2024-bjzbt **ORCID:** https://orcid.org/0000-0001-7852-497X Content not peer-reviewed by ChemRxiv. **License:** CC BY-NC-ND 4.0